November 1986 LIDS-P-1536

(Revised)

VARIABLE BACKGROUND BORN INVERSION BY WAVEFIELD BACKPROPAGATION[1]

by

Bernard C. Levy

Department of Electrical Engineering and Computer Science

Massachusetts Institute of Technology, Cambridge, MA 02139

and

Cengiz Esmersoy

Schlumberger-Doll Research, P.O. Box 307, Ridgefield, Connecticut 06877

[1]This work was supported in part by the Army Research Office under Grant No. DAAG29-84-K-0005, by the Air Force Office of Scientific Research under Grant No. AFOSR-85-0227, and by the National Science Foundation under Grant No. ECS-83-12921.

Abstract

The inverse scattering problem for an acoustic medium is formulated by using the variable background Born approximation. A constant density acoustic medium is probed by a wide-band point source, and the scattered field is observed along a curved receiver array located outside the region where the medium velocity is different from the assumed background velocity function. The solution that we propose relies on the introduction of a backpropagated field. This field is obtained by using a finite-difference scheme backwards in time to backpropagate into the medium the scattered field observed along the receiver array. The backpropagated field is imaged at the source travel times, giving an image of the same type as obtained by reverse-time finite-difference migration techniques. The gradient of this image is then taken along rays linking the source to points in the medium, and after scaling, this gives the reconstructed potential. To relate the reconstructed potential to the true scattering potential, we use high frequency asymptotics and an additional approximation introduced by Beylkin [1]. These approximations reduce the validity of our reconstruction procedure to the high wavenumber region. With these approximations, it is shown that at a given point, the reconstructed potential corresponds to the convolution of the true potential with a weighting function obtained by partially reconstructing an impulse from its projections inside a cone. The angular range of this cone is totally determined by the geometry of the receiver array, and by the relative location of the source with respect to the point that we consider. In the special case when the receiver array surrounds the domain where the scattering

potential is located, we find that within the Born approximation, the reconstructed potential recovers exactly the high wavenumber part of the Fourier transform of the true potential. It is expected that for a wide class of problems, the reconstruction technique described in this paper will be computationally more efficient that the generalized Radon transform (GRT) inversion method proposed by Beylkin, Miller and Oristaglio [1] - [3].

1. Introduction

The multidimensional inverse scattering problem for acoustic media has a wide range of applications in areas such as exploration geophysics [4], ultrasonic imaging [5], and nondestructive testing, among others. In this problem, the medium of interest is probed by sources located outside the medium and the scattered field is recorded at various locations. The objective is to reconstruct the velocity and density of the medium as functions of position. In this paper, we will assume for simplicity that the density of the medium is constant. Since the relation between the observations and the velocity function is nonlinear, the solution of the inverse problem must also be nonlinear. For one-dimensional (1-D) media, i.e. for media whose velocity function varies only with one space dimension, a number of exact inverse scattering procedures which rely either on integral or on differential equations have been proposed over the years. A discussion of these methods can be found in [6]. However for multidimensional media, exact inverse scattering methods are still at an early stage of development, and the methods which have been developed until now require experiment geometries which are rather unrealistic from a practical point of view.

This has motivated researchers to develop approximate direct inversion methods, which solve exactly a linearized form of the multidimensional inverse scattering problem. The Born and Rytov approximations [7] are the most commonly employed of these linearization techniques. Whether one should use one of these approximations instead of the other depends on the nature of the scatterers and on the experiment geometry. In this paper, we shall consider

the Born approximation. In this approximation, the object profile that we want to reconstruct is viewed as a small perturbation about an assumed background velocity model, and the scattered field is expressed linearly in terms of this perturbation. Physically, the Born approximation takes into account only the singly scattered waves; multiple scattered waves due to the velocity perturbations are neglected. Note however that the multiples due to the background model are included in the scattered field.

During the past few years, a number of solutions of the multidimensional Born inversion problem have been proposed for various observation geometries and background velocity models. The majority of these solutions assume a homogeneous background model. The zero-offset reflection geometry consisting of coincident sources and receivers was considered by Cohen and Bleistein [8] for a line aperture in two dimensions, and by Norton and Linzer [5] for plane, cylindrical and spherical apertures in three dimensions. More recently, Fawcett [9] formulated the zero-offset Born inversion problem as a tomographic problem, where the objective is to reconstruct a function from its projections along circles or spheres. The inversion method proposed by Cohen and Bleistein was also extended to the case of a stratified (1-D) background model in [10] and [11]. Raz [12] and Clayton and Stolt [13] considered the same experiment geometry as Cohen and Bleistein, but with unstacked data. In this geometry, some source and receiver arrays are located on the surface of the earth, and for each source the scattered field is recorded at all receivers rather than only at the coincident receiver. They showed that both the density and bulk modulus of the acoustic medium can be recovered with this experiment. Another interesting feature of Clayton and Stolt's paper is that

it assumes a variable background model, which is then taken into account by extrapolating the observed scattered field downwards into the medium of interest.

The solution of the multidimensional Born inversion problem which was proposed by Esmersoy and his colleagues [14]-[16] relies on a similar backpropagation principle. However, they considered a different scattering experiment, where the medium is probed by a single wide-band point or plane-wave source, and where the scattered field is measured along a curved receiver array located outside the region where the medium velocities differ from the background model. In this approach, the scattering potential is reconstructed by propagating the observed scattered field backwards in time with a finite-difference scheme, imaging this field either at zero time [15] or at the source travel times [14], [16], and then filtering the resulting image. Depending on whether the receiver array surrounds the scattering object or not, the reconstructed potential is an exact or approximate solution of the linearized inverse scattering problem. However, an important limitation of the results described in [14]-[16] is that they were restricted to the homogeneous background case.

The first complete solution of the variable background Born inversion problem was presented by Beylkin, Miller and Oristaglio [1] - [3], who formulated this problem as a generalized Radon transform (GRT) inversion problem, where the objective is to reconstruct a function from its projections along a set of curves whose geometry depends on the experiment and on the background model. The solution obtained by Beylkin and his colleagues is expressed in terms of a weighted backprojection operator summing the

contributions of the curves passing through a given point. This solution is quite general since it applies both to the case when the medium is probed by a single point source, and to the zero-offset and finite-offset geometries. Note however that the inverse GRT relies on high frequency asymptotics, and on an additional approximation which together have the effect that the reconstructed potential recovers only the rapid space variations of the true potential, or equivalently the high wavenumber part of its Fourier transform. Thus, the inverse GRT solves the variable background Born inversion problem only in a limited sense. Another limitation of the inverse GRT is that to obtain the weights appearing in the backprojection operator, one must use a ray tracing algorithm for every point along the receiver array where measurements are taken. The amount of computations required by this method is therefore quite large.

The objective of this paper is to extend the backpropagated field approach of [14]-[16] to the variable background case for the experiment where the medium is probed by a single wide-band point source. The computational procedure that we use to obtain the reconstructed potential is quite different from the inverse GRT, but the domain of validity of our reconstruction method is the same as that of the inverse GRT. In other words, the reconstructed potential recovers only the rapid space variations of the true potential, or equivalently the high wavenumber part of its Fourier transform. The first step in our approach is to filter the observed time traces and to use them as source wavelets for doublet sources located along the receiver array. For this source configuration, a finite difference scheme is used backwards in time to compute the backpropagated field inside the medium. This field is

then imaged at the source travel times, and the reconstructed potential is obtained by taking the gradient of this image along rays linking the source to points in the medium, and by scaling the resulting expression. To relate the reconstructed potential to the true potential, we use high frequency asymptotics as well as an additional approximation introduced by [1]. These approximations reduce the domain of validity of our inversion method to the high wavenumber region. In this context, it is shown that at a fixed point, the reconstructed potential is the convolution of the true potential with a weighting function obtained by partially reconstructing an impulse from its projection inside a cone. The angular range of this cone is totally determined by the geometry of the receiver array and by the location of the source with respect to the point that we consider. A consequence of this representation is that in the special case when the receiver array provides a total coverage of the scattering region, and within the domain of the validity of the Born approximation, our reconstruction procedure recovers exactly the high wavenumber part of the Fourier transform of the scattering potential.

The step of our reconstruction method which is the most demanding from a computational point of view is the computation of the backpropagated field with a finite-difference scheme. We expect that for a significant number of problems, this computation will be easier to perform than the ray tracing scheme which is required for every receiver by the inverse GRT.

This paper is organized as follows. In section 2, the velocity inversion problem is formulated within the Born approximation. The definition and implementation of the backpropagated field are discussed in section 3. Our reconstruction method is described in section 4, and a representation theorem

is obtained for the weighting function relating the reconstructed potential to the true potential. This representation relies on approximations which reduce the domain of validity of our reconstruction procedure to the high wavenumber region. The representation that we obtain shows that at a given point, the weighting function is the partial reconstruction of an impulse from its projections over a cone. The construction of this cone is examined in section 5, and is shown to depend only on the experiment geometry. Section 6 contains some conclusions and some thoughts about further extensions of our results.

2. Problem Description

Consider the scattering experiment described in Fig. 1. A constant density 2-D acoustic medium is probed by an impulsive point source located at $\underline{\eta}$ in the x-y plane. Since this 2-D medium is in fact a 3-D medium whose velocity function $c(\underline{x})$ does not vary with the third dimension z, the 2-D point source is in fact implemented by a line source parallel to the z axis. The scattered field is observed along a curved receiver array Γ, and in the following it is assumed that Γ is a smooth curve parameterized by the arc length s, $s \in I$.

Note that since we assume that the 2-D medium is probed by a line source, the experiment geometry described above is not totally realistic. In practice, it is much cheaper to use a point source to probe the medium. In this case the problem becomes a 2 1/2-D problem in the sense that although the velocity function $c(\underline{x})$ varies only with two space dimensions, the waves propagate in three dimensions. The geometrical spreading associated to the three-dimensional propagation of the waves needs to be taken explicitly into account in the inversion problem, and a detailed analysis showing how this can be done can be found in [17], and [14], section 2.6. However, to simplify our analysis, it will be assumed below that the medium is probed by a line source.

Then, the Fourier transform $P(\underline{x},\omega)$ of the pressure field satisfies

$$[\nabla^2+k^2n^2(\underline{x})]\ P(\underline{x},\omega) = -\delta(\underline{x}-\underline{\eta}) \qquad (2.1)$$

where $k = \omega/c$ is the wavenumber, and $n(\underline{x}) = c/c(\underline{x})$ is the refraction index of the medium measured with respect to some constant velocity c. Throughout this

paper, it will be assumed that $n(\underline{x})$ does not deviate significantly from a background index $n_0(\underline{x})$, so that

$$n^2(\underline{x}) = n_0^2(\underline{x}) + U(\underline{x}) \quad , \tag{2.2}$$

where the scattering potential $U(\underline{x})$ is small. In addition, we assume that $n_0(\bullet)$ is a smooth function and that $U(\bullet)$ has a bounded support V, which is completely located on the same side of Γ, as shown in Fig. 1. Substituting (2.2) inside (2.1), we can rewrite equation (2.1) as

$$[\nabla^2 + k^2 n_0^2(\underline{x})]\ P(\underline{x},\omega) = -\ \delta(\underline{x}-\underline{\eta}) - k^2 U(\underline{x})\ P(\underline{x},\omega) \tag{2.3}$$

where the operator $D_0 = \nabla^2 + k^2 n_0^2(\underline{x})$ appearing on the left-hand side of (2.3) is the background Helmoltz operator, and where the second term on the right-hand side can be viewed as a perturbation. The solution of (2.3) is given by

$$P(\underline{x},\omega) = P_0(\underline{x},\omega) + k^2 \int_V d\underline{x}'\, U(\underline{x}')P(\underline{x}',\omega)G_0(\underline{x},\underline{x}',\omega), \tag{2.4}$$

where the incident field $P_0(\underline{x},\omega)$ satisfies the unperturbed equation

$$D_0 P_0(\underline{x},\omega) = -\delta(\underline{x}-\underline{\eta}) \tag{2.5}$$

and where $G_0(\underline{x},\underline{x}',\omega)$ is the Green's function associated to D_0, i.e.

$$D_0 G_0(\underline{x},\underline{x}',\omega) = -\delta(\underline{x}-\underline{x}') \quad . \tag{2.6}$$

By comparing (2.5) and (2.6) we see that for the experiment geometry considered here, the incident field $P_0(\underline{x},\omega) = G_0(\underline{x},\underline{\eta},\omega)$.

The main feature of equation (2.4) is that it is <u>exact</u>, i.e. no approximations are involved up to this point. This equation is known as the Lippmann-Schwinger equation [18], and it puts in evidence the nonlinear relation existing between the potential $U(\underline{x})$ and the pressure field $P(\underline{x},\omega)$. In this paper, we will linearize this equation by using the <u>Born approximation</u>, whereby the total field $P(\underline{x},\omega)$ is approximated by the incident

field $P_0(\underline{x}, \omega) = G_0(\underline{x}, \underline{\eta}, \omega)$ inside the integral appearing in equation (2.4). In this case, the scattered field $P_s(\underline{x},\omega) = P(\underline{x},\omega) - P_0(\underline{x},\omega)$ can be expressed as

$$P_s(\underline{x},\omega) = k^2 \int_V d\underline{x}' U(\underline{x}') G_0(\underline{x},\underline{x}',\omega) G_0(\underline{x}',\underline{\eta},\omega) \ . \qquad (2.7)$$

Note that the Born approximation is valid only if the scattering potential $U(\bullet)$ is small both in magnitude and spatial extent ([19], Chapter 9). Then, the relation between $P_s(\bullet,\omega)$ and $U(\bullet)$ becomes <u>linear</u>, and the inverse problem that we shall consider in this paper consists in reconstructing $U(\underline{x})$ for $\underline{x} \in V$ from the observed scattered field $P_s(\underline{\xi},\omega)$ where $\underline{\xi} = \underline{\xi}(s)$ is located along the array Γ. Note that the receiver array Γ may not provide a total coverage of the domain V, so that in general $U(\underline{x})$ will only be partially reconstructed from the given observations.

Throughout this paper, we shall use the geometrical optics approximation

$$G_0(\underline{x},\underline{x}',\omega) \simeq \frac{e^{i\pi/4}}{k^{1/2}} a(\underline{x},\underline{x}') e^{ik\varphi(\underline{x},\underline{x}')} \qquad (2.8)$$

for points $\underline{x} \in V$, and for $\underline{x}' = \underline{\eta}$ or $\underline{x}' \in \Gamma$, and where for negative values of k, $k^{1/2} = i(-k)^{1/2}$. This approximation is a high-frequency approximation. Equivalently, it corresponds to assuming that the distance between the domain V where the scattering potential $U(\bullet)$ is located and the source and receivers is large when compared to the wavelengths used to probe the medium, so that

$$k|\underline{x}-\underline{x}'| >> 1 \qquad (2.9)$$

for $\underline{x} \in V$ and $\underline{x}' = \underline{\eta}$ or $\underline{x}' \in \Gamma$. In (2.8) $\varphi(\underline{x},\underline{x}')$ is the phase or travel time function and satisfies the eikonal equation

$$|\nabla_{\underline{x}} \varphi(\underline{x},\underline{x}')| = n_0(\underline{x}), \qquad (2.10)$$

and the amplitude $a(\underline{x},\underline{x}')$ obeys the transport equation

$$a\nabla^2_{\underline{x}}\varphi + 2\nabla_{\underline{x}}a\bullet\nabla_{\underline{x}}\varphi = 0 \qquad (2.11)$$

along the ray linking points $\underline{x}$ and $\underline{x}'$. For the special case when the background refraction index is constant, i.e. when $n_0(\underline{x}) = n_0$, we have $G_0(\underline{x},\underline{x}',\omega) = iH_0^{(1)}(kn_0|\underline{x}-\underline{x}'|)/4$ where $H_0^{(1)}(\bullet)$ denotes the Hankel function of order zero and type one, and the approximation (2.8) reduces to

$$G_0(\underline{x},\underline{x}',\omega) \simeq \frac{e^{i\pi/4}}{k^{1/2}} \frac{1}{2(2\pi n_0|\underline{x}-\underline{x}'|)^{1/2}} e^{ikn_0|\underline{x}-\underline{x}'|} . \qquad (2.12)$$

Then, substituting the approximation (2.8) inside (2.7), and setting $\underline{x} = \underline{\xi}$, we obtain

$$\frac{1}{ik} P_s(\underline{\xi},\omega) = \int_V d\underline{x}'U(\underline{x}')A(\underline{x}',\underline{\xi})e^{ik\Phi(\underline{x}',\underline{\xi})} \qquad (2.13)$$

where

$$A(\underline{x},\underline{\xi}) = a(\underline{x},\underline{\xi})a(\underline{x},\underline{\eta}) \qquad (2.14a)$$

$$\Phi(\underline{x},\underline{\xi}) = \varphi(\underline{x},\underline{\xi}) + \varphi(\underline{x},\underline{\eta}) . \qquad (2.14b)$$

Denoting

$$F(\underline{\xi},k) = P_s(\underline{\xi},\omega)/ik \qquad (2.15)$$

and letting $f(\underline{\xi},r)$ be the inverse Fourier transform of $F(\underline{\xi},k)$ with respect to k, we find that

$$\begin{aligned} f(\underline{\xi},r) &= -\int_0^{r/c} p_s(\underline{\xi},\tau)d\tau \\ &= \int_V d\underline{x}'U(\underline{x}')A(\underline{x}',\underline{\xi})\delta(r-\Phi(\underline{x}',\underline{\xi})) \end{aligned} \qquad (2.16)$$

where the time function $p_s(\underline{\xi},t)$ is the scattered field observed at $\underline{\xi}$.

The identity (2.16) indicates that $f(\underline{\xi},r)$ can be viewed as a weighted projection of the potential $U(\bullet)$ along the curve $\Phi(\underline{x},\underline{\xi}) = r$, and that $f(\underline{\xi},r)$ is obtained by integrating the scattered field $p_s(\underline{\xi},\bullet)$. Thus, the inverse

scattering problem that we consider here can be formulated as a generalized Radon transform (GRT) inversion problem. This was the point of view adopted by Beylkin, Miller and Oristaglio [1]-[3], who were then able to obtain a backprojection operator to reconstruct the potential $U(\bullet)$ partially from its projections $f(\underline{\xi},\underline{r})$ where $\underline{\xi} \in \Gamma$ and $0 \leq r < \infty$. However, one disadvantage of the GRT inversion method is that to implement the backprojection operator, it requires the computation of the amplitude $a(\underline{x},\underline{\xi})$ and phase $\varphi(\underline{x},\underline{\xi})$ for every point $\underline{x}$ in the medium and every receiver $\underline{\xi} \in \Gamma$, as well as the computation of $a(\underline{x},\underline{\eta})$ and $\varphi(\underline{x},\underline{\eta})$ for all points $\underline{x}$, where the position $\underline{\eta}$ of the source is fixed. This amount of computations is very large, and the inverse GRT is therefore very costly to implement.

The objective of this paper is to obtain an alternative reconstruction method, whose computational requirements will be smaller for a significant class of problems.

3. The Backpropagated Field

The inversion method that we propose relies on the concept of backpropagated field, which was first introduced in the context of holographic imaging by Porter [20]. This idea was subsequently used by Bojarski [21] and Esmersoy [14] to study inverse source and inverse scattering problems, and it was applied to the solution of the constant background inversion problem for an impulsive point source and for a plane wave source in [15] and [16], respectively. The migration methods [22] - [24] which are currently used in exploration geophysics also rely on the concept of extrapolated field to image the main reflectors contained in a scattering medium. By migration we mean here a technique which is used to image the discontinuities of the scattering

potential $U(\underline{x})$. Migration differs from inversion by the fact that in migration the objective is only to detect discontinuities of $U(\underline{x})$, whereas inversion methods seek to obtain some precise quantitative information, perhaps only partial, about the values of the function $U(\underline{x})$ or of its Fourier transform.

For the experiment geometry considered here, the backpropagated field is defined as

$$P_e(\underline{x},\omega) = \int_I ds\ W(\omega)P_s(\underline{\xi},\omega)\ \nabla_{\underline{\xi}}G_0^*(\underline{x},\underline{\xi},\omega)\bullet\hat{\nu}(\underline{\xi}) \qquad (3.1)$$

where $W(\omega)$ is a filter to be determined later, and where $\hat{\nu}(\underline{\xi})$ is the unit vector perpendicular to Γ at point $\underline{\xi}$, oriented in the outwards direction, as shown in Fig. 2. Note that in integral (3.1), the receiver position $\underline{\xi} = \underline{\xi}(s)$ is a function of the arc length s, but for simplicity this dependence will not be indicated explicitly in the mathematical expressions that we shall consider below, except at places where our analysis will need to take this dependence into account. Here, $\nabla_{\underline{\xi}}G_0(\underline{x},\underline{\xi},\omega)\bullet\hat{\nu}(\underline{\xi})$ denotes the Green's function of a doublet, i.e. it can be implemented by two impulsive sources of opposite signs located perpendicularly across the curve Γ at a very small distance from each other, as shown in Fig. 2. The fact that we select the complex conjugate of $\nabla_{\underline{\xi}}G_0(\underline{x},\underline{\xi},\omega)$ indicates that the waves propagate <u>anticausally</u> (backwards in time), since we want to reconstruct the pressure field inside the medium at earlier times.

The expression (3.1) for the backpropagated field $P_e(\underline{x},\omega)$ has the following physical interpretation: $P_e(\underline{x},\omega)$ is the acoustic field which is obtained by replacing the receivers along the curve Γ by doublet sources, and

by exciting the doublet located at point $\underline{\xi} \in \Gamma$ with the source wavelet $W(\omega)\, P_s(\underline{\xi}, \omega)$. This source wavelet is obtained by passing the scattered field observed at $\underline{\xi}$ through the filter $W(\omega)$. From a practical point of view, $P_e(\underline{x}, \omega)$ can be computed in a number of ways. The method that we propose consists in observing from (3.1) that $P_e(\underline{x}, \omega)$ satisfies

$$D_0 P_e(\underline{x}, \omega) = 0 \tag{3.2}$$

for $\underline{x} \notin \Gamma$. Then if we specify an appropriate boundary condition for this equation, the backpropagated field $p_e(\underline{x}, t)$, where $p_e(\underline{x}, t)$ denotes the inverse Fourier transform of $P_e(\underline{x}, \omega)$, can be computed backwards in time by using a finite-difference scheme of the type described in [25]. Note that except for the introduction of the filter $W(\omega)$, the procedure described above for computing $p_e(\underline{x}, t)$ is identical to the reverse-time finite difference migration method for unstacked data which was proposed in [26], where the boundary condition

$$p_e(\underline{\xi}, t) = p_s(\underline{\xi}, t) \tag{3.3}$$

for $\underline{\xi} \in \Gamma$ and $t \geq 0$ was selected.

The only element that has been left unspecified above is the choice of boundary conditions for $p_e(\underline{x}, t)$. Strictly speaking, to obtain an exact boundary condition for $P_e(\underline{x}, \omega)$ one would need to use the expression (3.1) to specify the value of $p_e(\underline{x}, t)$ over a boundary $\tilde{\Gamma}$ located close to the array Γ. However, it is more convenient to note that when equation (3.1) for $P_e(\underline{x}, \omega)$ is equated to expression (3.11) below, and when Γ surrounds the domain V, it was shown by Esmersoy in [14], pp. 99-105 that

$$p_e(\underline{\xi}, t) = p_s^f(\underline{\xi}, t) \tag{3.4a}$$

for $\underline{\xi} \in \Gamma$ and

$$t > \max_{\underline{x} \in V} (\varphi(\underline{x},\underline{\eta}) - \varphi(\underline{x},\underline{\xi})) \ , \tag{3.4b}$$

where $p_s^f(\underline{\xi},t)$ denotes the inverse Fourier transform of the filtered scattered field $W(\omega)P_s(\underline{\xi},\omega)$.

The identity (3.4a) specifies a boundary condition for the extrapolated field $p_e(\underline{x},t)$ over the time window (3.4b). Since the inversion method that we propose in section 4 requires the knowledge of $p_e(\underline{x},t)$ only at $t = \varphi(\underline{x},\underline{\eta})$, where $\varphi(\underline{x}.\underline{\eta})$ is the travel time from the source $\underline{\eta}$ to point $\underline{x} \in V$, the time window (3.4b) is in general sufficient to compute the values of $p_e(\underline{x},t)$ that we need. In addition, the boundary condition (3.4a) is so simple that even when Γ does not surround the domain V, it may be worth using it to compute an approximation to $p_e(\underline{x},t)$. This scheme has given good results in [14], [16]. However, as indicated above, a more rigorous method would need to start from the definition (3.1) of $P_e(\underline{x},\omega)$.

A representation of the backpropagated field which will be useful in subsequent derivations can be obtained by noting that within the geometrical optics approximation

$$\nabla_{\underline{\xi}} G_0(\underline{x},\underline{\xi},\omega) = \frac{e^{i\pi/4}}{k^{1/2}} (\nabla_{\underline{\xi}} a(\underline{x},\underline{\xi}) + ika(\underline{x},\underline{\xi}) \nabla_{\underline{\xi}} \varphi(\underline{x},\underline{\xi})) e^{ik\varphi(\underline{x},\underline{\xi})} \tag{3.5}$$

Then, if we make the additional approximation

$$|\nabla_{\underline{\xi}} a(\underline{x},\underline{\xi})| << |ka(\underline{x},\underline{\xi})| \tag{3.6}$$

which is of the same nature as the geometrical optics approximation, we find that

$$\nabla_{\underline{\xi}} G_0(\underline{x},\underline{\xi},\omega) \simeq -k^{1/2} e^{-i\pi/4} a(\underline{x},\underline{\xi}) \nabla_{\underline{\xi}} \varphi(\underline{x},\underline{\xi}) e^{ik\varphi(\underline{x},\underline{\xi})} \ . \tag{3.7}$$

The vector $\hat{v}(\underline{x},\underline{\xi}) \overset{\Delta}{=} \nabla_{\underline{\xi}}\varphi(\underline{x},\underline{\xi})$ is tangent to the ray linking $\underline{x}$ and $\underline{\xi}$, as shown in Fig. 2, and

$$|\hat{v}(\underline{x},\underline{\xi})| = n_0(\underline{\xi}), \tag{3.8}$$

so that

$$\nabla_{\underline{\xi}}G_0(\underline{x},\underline{\xi},\omega)\cdot\hat{\upsilon}(\underline{\xi}) \simeq -k^{1/2}e^{-i\pi/4}n_0(\underline{\xi})\cos\beta(\underline{x},\underline{\xi})a(\underline{x},\underline{\xi})e^{ik\varphi(\underline{x},\underline{\xi})}$$

$$= ikn_0(\underline{\xi})\cos\beta(\underline{x},\underline{\xi})G_0(\underline{x},\underline{\xi},\omega) \ , \tag{3.9}$$

where $\beta(\underline{x},\underline{\xi})$ is the angle between the normal vector $\hat{\upsilon}(\underline{\xi})$ and $\hat{v}(\underline{x},\underline{\xi})$. Substituting (3.9) inside (3.1), and taking into account the definition (2.15) of $F(\underline{x},k)$, this gives the following expression for the extrapolated field

$$P_e(\underline{x},\omega) = k^2W(\omega)\int_I ds\ F(\underline{\xi},k)n_0(\underline{\xi})\cos\beta(\underline{x},\underline{\xi})G_0^*(\underline{x},\underline{\xi},\omega) \tag{3.10}$$

which will be used in next section.

It is worth noting that the definition (3.1) of the backpropagated field differs from the definition selected in [14] and [16], where $P_e(\underline{x},\omega)$ was given by the Kirchhoff integral

$$P_e(\underline{x},\omega) = W(\omega)\int_I ds[P_s(\underline{\xi},\omega)\nabla_{\underline{\xi}}G_0^*(\underline{x},\underline{\xi},\omega)$$

$$- \nabla_{\underline{\xi}}P_s(\underline{\xi},\omega)G_0^*(\underline{x},\underline{\xi},\omega)]\cdot\hat{\upsilon}(\underline{\xi}) \ . \tag{3.11}$$

The motivation for considering the expression (3.1) instead of (3.8) is that it is simpler, so that our subsequent derivations will be easier to follow. There is however no practical reason why (3.1) should be used instead of (3.11). An important difference between (3.1) and (3.11) is that the definition (3.1) requires only the knowledge of the scattered field $P_s(\underline{\xi},\omega)$ along the receiver array Γ, whereas (3.11) requires also the knowledge of the normal derivative $\frac{\partial}{\partial n}P_s(\underline{\xi},\omega)$ along Γ. Since this derivative cannot usually be

measured, it may appear at first sight that the definition (3.11) cannot be implemented directly. However, as was already observed above, it was shown by Esmersoy [14] that with the definition (3.11), $p_e(\underline{x},t)$ can be computed in the time domain by using the homogeneous equation (3.2) with the boundary condition (3.4), so that the normal derivative $\frac{\partial}{\partial n} P_s(\underline{\xi},\omega)$ is not needed.

An argument which indicates that the definitions (3.1) and (3.11) are approximately equivalent is as follows. First, substitute the approximations

$$P_s(\underline{\xi},\omega) = k^{r_s} a_s(\underline{\xi}) e^{ik\varphi_s(\underline{\xi})} \tag{3.12a}$$

$$G_0(\underline{x},\underline{\xi},\omega) = k^{r_0} a(\underline{x},\underline{\xi}) e^{ik\varphi(\underline{x},\underline{\xi})} \tag{3.12b}$$

inside (3.11), and take into account (3.9), so that

$$\frac{\partial}{\partial n} P_s(\underline{\xi},\omega) = ik^{r_s+1} n_0(\underline{\xi}) \cos\beta_s(\underline{\xi}) P_s(\underline{\xi},\omega) \tag{3.13a}$$

$$\frac{\partial}{\partial n} G_0(\underline{x},\underline{\xi},\omega) = ik^{r_0+1} n_0(\underline{\xi}) \cos\beta(\underline{x},\underline{\xi}) G_0(\underline{x},\underline{\xi},\omega) \tag{3.13b}$$

where $\beta_s(\underline{\xi})$ and $\beta(\underline{x},\underline{\xi})$ denote respectively the angles that $\nabla_{\underline{\xi}}\varphi_s(\underline{\xi})$ and $\nabla_{\underline{\xi}}\varphi(\underline{x},\underline{\xi})$ make with the normal to Γ. The integrals along Γ of the first and second term in (3.11) are now expressed as

$$E_1 = -ik^r \int_I ds\; n_0(\underline{\xi}) a_s(\underline{\xi}) a^*(\underline{x},\underline{\xi}) \cos\beta(\underline{x},\underline{\xi}) e^{ik(\varphi_s(\underline{\xi})-\varphi(\underline{x},\underline{\xi}))} \tag{3.14a}$$

$$E_2 = -ik^r \int_I ds\; n_0(\underline{\xi}) a_s(\underline{\xi}) a^*(\underline{x},\underline{\xi}) \cos\beta_s(\underline{\xi}) e^{ik(\varphi_s(\underline{\xi})-\varphi(\underline{x},\underline{\xi}))} \tag{3.14b}$$

where $r = r_0 + r_s + 1$. The only difference between these two integrals is the weighting factors $\cos\beta(\underline{x},\underline{\xi})$ and $\cos\beta_s(\underline{\xi})$ which appear in (3.14a) and (3.14b) respectively. If the method of stationary phase is used to evaluate these integrals, we find that the stationary points are given by

$$(\nabla_{\underline{\xi}}\varphi_s(\underline{\xi}) - \nabla_{\underline{\xi}}\varphi(\underline{x},\underline{\xi})).\hat{t}(\underline{\xi}) = 0 \tag{3.15}$$

where $\hat{t}(\underline{\xi})$ denotes the unit vector tangent to the array Γ at point $\underline{\xi}$. But $\nabla_{\underline{\xi}}\varphi_s(\underline{\xi})$ and $\nabla_{\underline{\xi}}\varphi(\underline{x},\underline{\xi})$ satisfy the eikonal equation and have therefore the same magnitude $n_0(\underline{\xi})$. In addition, they are both oriented in the outward direction with respect to Γ, so that at a stationary point we must have

$$\nabla_{\underline{\xi}}\varphi_s(\underline{\xi}) = \nabla_{\underline{\xi}}\varphi(\underline{x},\underline{\xi}) \tag{3.16}$$

which in turn implies that

$$\cos\beta_s(\underline{\xi}) = \cos\beta(\underline{x},\underline{\xi}) \tag{3.17}$$

Thus, at stationary points of (3.14a) and (3.14b) the weighting functions appearing in the two integrals are equal, so that E_1 and E_2 make equal contributions to the leading order asymptotic expansion of $P_e(\underline{x},\omega)$. Consequently, except for a factor 2 which can be incorporated in $W(\omega)$, the expressions (3.1) and (3.11) are approximately the same. Note, however, that our analysis is only approximate since it relies on high frequency asymptotics. It turns out that there exist several special cases for which the two terms in (3.11) are exactly equal. This is the case for example when the background medium is constant and the receiver Γ is a straight line [19].

4. Inversion Method

4.1 Reconstruction Technique

The inversion procedure that we propose is just an extension of a method which was developed earlier by Esmersoy [14] for solving the linearized inversion problem for a point source with a constant background. The first step in our method is, for every point $\underline{x}$ in the medium, to image the backpropagated field $p_e(\underline{x},t)$ at the source travel time $t = \varphi(\underline{x},\underline{\eta})/c$. Here $\varphi(\underline{x},\underline{\eta})/c$ represents the time needed for waves originating from the source $\underline{\eta}$ to

reach $\underline{x}$. This gives the image

$$O(\underline{x}) = p_e(\underline{x}, \frac{1}{c}\varphi(\underline{x},\underline{\eta})) = \frac{1}{2\pi}\int_{-\infty}^{\infty} d\omega\ P_e(\underline{x},\omega)e^{-i\frac{\omega}{c}\varphi(\underline{x},\underline{\eta})} \tag{4.1}$$

The image $O(\underline{x})$ can be viewed as the migrated image obtained by applying the source travel-time imaging rule to the extrapolated field (see [26] for the description of a migration technique based on this principle).

Then, changing the integration variable from ω to $k=\omega/c$, taking into account the representation (3.10) for $P_e(\underline{x},\omega)$ and identities (2.13), (2.15), and using the geometrical optics approximation for $G_0(\bullet,\bullet,\omega)$, we obtain

$$O(x) = \int_V d\underline{x}'\ N(\underline{x},\underline{x}')U(\underline{x}') \quad , \tag{4.2}$$

where

$$N(\underline{x},\underline{x}') = \frac{c}{2\pi}\int_{-\infty}^{\infty} dk\ k^{3/2}e^{-i\pi/4}W(\omega)\int_I ds\ n_0(\underline{\xi})\cos\beta(\underline{x},\underline{\xi})\cdot$$
$$\bullet\ A(\underline{x}',\underline{\xi})\ a(\underline{x},\underline{\xi})e^{ik[\Phi(\underline{x}',\underline{\xi})-\Phi(\underline{x},\underline{\xi})]} \quad . \tag{4.3}$$

Let now

$$\hat{U}(\underline{x}) = \frac{1}{a(\underline{x},\underline{\eta})}\nabla_{\underline{x}}O(\underline{x})\bullet\nabla_{\underline{x}}\varphi(\underline{x},\underline{\eta}) \tag{4.4}$$

be the reconstructed value of the potential $U(\underline{x})$. Since the vector $\nabla_{\underline{x}}\varphi(\underline{x},\underline{\eta})$ is tangent to the ray linking the source $\underline{\eta}$ to point $\underline{x}$, and has magnitude $n_0(\underline{x})$, this value is obtained by taking the gradient of the migrated image $O(\underline{x})$ in the direction of the ray linking $\underline{\eta}$ to $\underline{x}$, and by scaling the resulting expression with $n_0(\underline{x})/a(\underline{x},\underline{\eta})$. The scaling by $n_0(\underline{x})/a(\underline{x},\underline{\eta})$ is needed to take dispersion effects into account. Then, from (4.2) we find that

$$\hat{U}(\underline{x}) = \int_V d\underline{x}'M(\underline{x},\underline{x}')U(\underline{x}') \tag{4.5}$$

where

$$M(\underline{x},\underline{x}') = \frac{1}{a(\underline{x},\underline{\eta})}\nabla_{\underline{x}}N(\underline{x},\underline{x}')\bullet\nabla_{\underline{x}}\varphi(\underline{x},\underline{\eta}) \quad . \tag{4.6}$$

Our objective in the remainder of this section will be to obtain a simple representation for $M(\underline{x},\underline{x}')$, which will be used to show that the reconstructed potential $\hat{U}(\underline{x})$ is a good approximation of $U(\underline{x})$.

4.2 Representation of $M(\underline{x},\underline{x}')$

The starting point in our derivation of a representation for $M(\underline{x},\underline{x}')$ is the expression (4.6), where $N(x,x')$ is given by (4.3). To evaluate $\nabla_{\underline{x}} N(\underline{x},\underline{x}')$, we assume that

$$|\nabla_{\underline{x}}(\cos\beta(\underline{x},\underline{\xi})a(\underline{x},\underline{\xi}))| \ll |k\cos\beta(\underline{x},\underline{\xi})a(\underline{x},\underline{\xi})\nabla_{\underline{x}}\Phi(\underline{x},\underline{\xi})| \ , \tag{4.7}$$

which, again, is an approximation of the same type as the geometrical optics approximation. This gives

$$\nabla_{\underline{x}} N(\underline{x},\underline{x}')\cdot\nabla_{\underline{x}}\varphi(\underline{x},\underline{\eta}) \simeq -\frac{c}{2\pi}\int_{-\infty}^{\infty} dk\, k^{5/2}\, e^{i\pi/4} W(\omega) \int_I ds\, n_0(\underline{\xi})\cos\beta(\underline{x},\underline{\xi})$$
$$\cdot A(\underline{x}',\underline{\xi})a(\underline{x},\underline{\xi})\nabla_{\underline{x}}\Phi(\underline{x},\underline{\xi})\cdot\nabla_{\underline{x}}\varphi(\underline{x},\underline{\eta})e^{ik[\Phi(\underline{x}',\underline{\xi}) - \Phi(\underline{x},\underline{\xi})]} \ . \tag{4.8}$$

Next, we note that

$$\nabla_{\underline{x}}\Phi(\underline{x},\underline{\xi}) = \hat{u}(\underline{x},\underline{\xi}) + \hat{u}_i(\underline{x}) \ , \tag{4.9}$$

where the vectors

$$\hat{u}_i(\underline{x}) \overset{\Delta}{=} \nabla_{\underline{x}}\varphi(\underline{x},\underline{\eta}) \tag{4.10a}$$

$$\hat{u}(\underline{x},\underline{\xi}) \overset{\Delta}{=} \nabla_{\underline{x}}\varphi(\underline{x},\underline{\xi}) \tag{4.10b}$$

are tangent to the rays linking $\underline{\eta}$ to $\underline{x}$ and $\underline{\xi}$ to $\underline{x}$, respectively, as shown in Fig. 2. These vectors are such that

$$|\hat{u}_i(\underline{x})| = |\hat{u}(\underline{x},\underline{\xi})| = n_0(\underline{x}) \ , \tag{4.11}$$

and in the following the angular arguments of $\hat{u}_i(\underline{x})$ and $\hat{u}(\underline{x},\underline{\xi})$ will be denoted

by $\theta_i(\underline{x})$ and $\theta(\underline{x},\underline{\xi})$, respectively. Thus

$$\nabla_{\underline{x}}\Phi(\underline{x},\underline{\xi})\bullet\nabla_{\underline{x}}\varphi(\underline{x},\underline{\eta}) = n_0^2(\underline{x})(1 + \cos\alpha(\underline{x},\underline{\xi})), \tag{4.12}$$

where $\alpha(\underline{x},\underline{\xi}) \overset{\Delta}{=} \theta(\underline{x},\underline{\xi}) - \theta_i(\underline{x})$ is the angle between the vectors $\hat{u}(\underline{x},\underline{\xi})$ and $\hat{u}_i(\underline{x})$. Then, by combining (4.6), (4.8) and (4.12), we obtain

$$M(\underline{x},\underline{x}') = -\frac{cn_0^2(\underline{x})}{2\pi a(\underline{x},\underline{\eta})}\int_{-\infty}^{\infty} dk\, k^{5/2}e^{i\pi/4}W(\omega)\int_I ds\, n_0(\underline{\xi})\cos\beta(\underline{x},\underline{\xi})\bullet$$
$$(1 + \cos\alpha(\underline{x},\underline{\xi}))\, A(\underline{x}',\underline{\xi})a(\underline{x},\underline{\xi})e^{ik[\Phi(\underline{x}',\underline{\xi}) - \Phi(\underline{x},\underline{\xi})]}. \tag{4.13}$$

This expression can be simplified further if, following Beylkin [1], we make the following approximation

$$A(\underline{x}',\underline{\xi}) \simeq A(\underline{x},\underline{\xi}) \tag{4.14a}$$

$$\Phi(\underline{x}',\underline{\xi}) \simeq \Phi(\underline{x},\underline{\xi}) + \nabla_{\underline{x}}\Phi(\underline{x},\underline{\xi})\bullet(\underline{x}'-\underline{x}) \tag{4.14b}$$

for $\underline{x}$, $\underline{x}' \in V$ and $\underline{\xi} \in \Gamma$. A rigorous analysis of this approximation in terms of pseudodifferential operators was proposed by Beylkin. In this context, it was shown that (4.14) has the effect of retaining the singular component of $M(\underline{x},\underline{x}')$, which is nonzero only when $\underline{x}'$ is in the vicinity of $\underline{x}$, and of neglecting the smooth components of $M(\underline{x},\underline{x}')$. When the smooth components of $M(\underline{x},\underline{x}')$ are dropped from identity (4.5), only the rapid space variations of $\hat{U}(\underline{x})$, such as the location and size of discontinuities, can be related to those of $U(\underline{x})$. Equivalently, in the Fourier domain, only the high wavenumber part of the Fourier transform of $\hat{U}(\underline{x})$ is related to that of $U(\underline{x})$. Another interpretation of appromixation (4.14) which is perhaps more appealing from a physical point of view consists in observing that when V is in the far field of the receiver array Γ, the distance $|\underline{x} - \underline{x}'|$ between points $\underline{x}$, $\underline{x}' \in V$ is small

with respect to $|\underline{x} - \underline{\xi}|$ where $\underline{\xi}\epsilon\Gamma$, and in this case the Taylor series expansion (4.14) is justified. Note however that for geophysical surveys, it cannot always be assumed that V is in the field of Γ, and in this case the justification of (4.14) proposed by Beylkin is more appropriate.

The end effect of (4.14) is that (4.13) takes the form

$$M(\underline{x},\underline{x}') = -\frac{cn_0^2(\underline{x})}{2\pi}\int_{-\infty}^{\infty} dk\, k^{5/2} e^{i\pi/4} W(\omega) \int_I ds\, n_0(\underline{\xi})\cos\beta(\underline{x},\underline{\xi})\bullet$$
$$(1 + \cos\alpha(\underline{x},\underline{\xi}))\, a^2(\underline{x},\underline{\xi}) e^{ik\nabla_{\underline{x}}\Phi(\underline{x},\underline{\xi})\bullet(\underline{x}'-\underline{x})} . \qquad (4.15)$$

Now, consider an infinitesimal ray tube originating from $\underline{x}$ and centered around the ray linking $\underline{x}$ to $\underline{\xi} \in \Gamma$, as shown in Fig. 3. If $\underline{\xi}'$is an arbitrary point along the ray linking $\underline{x}$ to $\underline{\xi}$, and if $d\sigma$ and $d\sigma'$ are the cross-sections of the tube at $\underline{\xi}$ and $\underline{\xi}'$ respectively, we have [27]

$$n_0(\underline{\xi})a^2(\underline{x},\underline{\xi})\, d\sigma = n_0(\underline{\xi}')\, a^2(\underline{x},\underline{\xi}')d\sigma' . \qquad (4.16)$$

But $d\sigma$ can be expressed in terms of the element ds of arc length along Γ as

$$d\sigma = ds\, \cos\beta(\underline{x},\underline{\xi}) . \qquad (4.17)$$

Furthermore, if $d\theta$ is the angular span of the tube at $\underline{x}$, and if $\underline{\xi}'$ is located at a very small distance ρ from $\underline{x}$, we have

$$n_0(\underline{\xi}') \simeq n_0(\underline{x}) \qquad (4.18a)$$

$$d\sigma' = \rho d\theta \qquad (4.18b)$$

$$a^2(\underline{x},\underline{\xi}') \simeq \frac{1}{8\pi n_0(\underline{x})\rho} \qquad (4.18c)$$

where to obtain (4.18c) we have used the asymptotic form (2.10) of a homogeneous Green's function, and the fact that in the vicinity of $\underline{x}$, the medium is locally homogeneous. This gives

$$n_0(\underline{\xi})a^2(\underline{x},\underline{\xi})\cos\beta(\underline{x},\underline{\xi})\, ds = \frac{1}{8\pi} d\theta , \qquad (4.19)$$

so that $M(\underline{x},\underline{x}')$ can be rewritten as

$$M(\underline{x},\underline{x}') = -\frac{cn_0^2(\underline{x})}{16\pi^2}\int_{-\infty}^{\infty} dk\, k^{5/2}\, e^{i\pi/4} W(\omega) \int_I ds\, (1+\cos\alpha(\underline{x},\underline{\xi})).$$

$$\cdot \frac{d\theta}{ds}(\underline{x},\underline{\xi}) e^{ik\underline{v}_{\underline{x}}\Phi(\underline{x},\underline{\xi})\cdot(\underline{x}'-\underline{x})} \quad . \tag{4.20}$$

Now, consider the change of variables

$$T(\underline{x}) : (s,k) \longrightarrow \underline{p} = k\underline{v}_{\underline{x}}\Phi(\underline{x},\underline{\xi}(s)) \tag{4.21}$$

and let $C(\underline{x})$ be the image of I x IR under this transformation. Since $\underline{p}$ depends linearly on k, the domain $C(\underline{x})$ is a cone whose span varies with $\underline{x}$. It was shown by Beylkin [1] that the Jacobian of this transformation is given by

$$J(\underline{x},s,k) = |k| n_0^2(\underline{x})(1+\cos\alpha(\underline{x},\underline{\xi}(s)))\frac{d\theta}{ds}(\underline{x},\underline{\xi}(s)) \quad . \tag{4.22}$$

Consequently, if we select

$$W(\omega) = -\frac{4e^{-i\pi/4}}{c|k|k^{1/2}}, \tag{4.23}$$

the weighting function M(x,x') can be expressed as

$$M(\underline{x},\underline{x}') = \frac{1}{(2\pi)^2}\int_{C(\underline{x})} d\underline{p}\, e^{i\underline{p}\cdot(\underline{x}'-\underline{x})}, \tag{4.24}$$

which is the desired representation for $M(\underline{x},\underline{x}')$.

From (4.24), we see that when $M(\underline{x},\underline{x}')$ is viewed as a function of $\underline{d} = \underline{x}'-\underline{x}$ parametrized by $\underline{x}$, it is the inverse Fourier transform of the characteristic function

$$\chi(\underline{x},\underline{p}) = \begin{cases} 1 & \text{for } \underline{p} \in C(\underline{x}) \\ 0 & \text{otherwise} \end{cases} \quad . \tag{4.25}$$

This shows that $M(\underline{x},\underline{x}')$ is a partial reconstruction of an impulse, where the cone $C(\underline{x})$ specifies the range of available projections. In the special case when $C(\underline{x}) = IR^2$, which corresponds to an experiment geometry where the

receiver array Γ surrounds V, we have $M(\underline{x},\underline{x}') = \delta(\underline{x}-\underline{x}')$, so that in this case we can conclude that

$$\hat{U}(\underline{x}) = U(\underline{x}). \tag{4.26}$$

The identity (4.26) seems to suggest that our inversion procedure recovers exactly the scattering potential $U(\underline{x})$. It is worth remembering at this point that identity (4.26), as well as the representation (4.24) for the kernel $M(\underline{x},\underline{x}')$ are only valid within the limits imposed by the approximations we have made. These approximations are of course the Born approximation, but also the geometrical optics expansion (2.8) and approximation (4.14). It turns out that these last two approximations impose some very severe restrictions on our interpretation of (4.24) and (4.26). As we observed above, approximation (4.14) is automatically satisfied if V is in the far field of Γ. Otherwise, as was shown by Beylkin [1], the smooth components of $M(\underline{x},\underline{x}')$ are neglected, so that expression (4.25) for the Fourier transform of $M(\underline{x},\underline{x}')$ is only valid when the wavevector $\underline{p}$ is large, and therefore identity (4.26) should be interpreted in the Fourier domain as

$$\hat{U}(\underline{p}) = U(\underline{p}) \tag{4.27}$$

for large $\underline{p}$.

It will be shown now that the geometrical optics expansion (2.8) imposes similar restrictions on the validity of relations (4.24) and (4.26). To see this, note that since k has been assumed large, there exists some constant r such that $|k| \geq r$. Then the transform variable $\underline{p}$ defined by (4.21) takes values over a set $C_r(\underline{x})$ which is the image of $I \times \{k: |\geq r\}$ under $T(\underline{x})$. This set is obtained by subtracting from the cone $C(\underline{x})$ a region in the vicinity of $\underline{p} = 0$. The set $C_r(\underline{x})$ is characterized in detail in section 5. The main

aspect of this characterization is that although k is bounded away from zero, the magnitude of $p = |\underline{p}|$ of the wavevector $\underline{p}$ is not necessarily nonzero, since it depends on the length of the vector $\nabla_{\underline{x}}\Phi(\underline{x},\underline{\xi})$ given by (4.9). In fact, when the receiver $\underline{\xi}$ is located on the other side of V with respect to the source $\underline{\eta}$ which may occur for a vertical seismic profiling experiment where the source is on the surface of the earth and the receivers along a vertical borehole, the length of $\nabla_{\underline{x}}\Phi(\underline{x},\underline{\xi})$ is close to zero. Nevertheless, the constraint $|k| \geq r$ has the effect that the Fourier transform relation (4.25) for $M(\underline{x},\underline{x}')$ is restricted to $\underline{p} \in C_r(\underline{x})$. In the case of complete receiver coverage, this also implies that equality (4.27) between the Fourier transforms of $U(\underline{x})$ and $\hat{U}(\underline{x})$ holds primarily for large values of $\underline{p}$.

Thus, both approximations (4.14) and the high frequency asymptotics that we have employed have the effect of restricting the validity of our inversion method to the high wavenumber region.

To interpret the filter $W(\omega)$ which is used to process the scattered field $P_s(\underline{\xi},\omega)$, also observe that since $k = \omega/c$, we can rewrite

$$W(\omega) = 4c^{1/2} \frac{1}{(-i\omega)} \frac{1}{(-i\omega)^{1/2}} , \qquad (4.28)$$

so that $W(\omega)$ corresponds to an integration followed by a square-root integration.

4.3 Summary

To conclude, let us review our reconstruction procedure step by step.

1) First, the scattered field $P_s(\underline{\xi},\omega)$ observed at the receivers is filtered with $W(\omega)$, which requires performing an integration, followed by a square-root integration.

2) The receivers are replaced by doublet sources, and the filtered time traces are used as source wavelets. Then, for this distribution of sources, the backpropagated field $p_e(\underline{x},t)$ is computed by a finite-difference scheme.

3) The backpropagated field $p_e(\underline{x},t)$ is imaged at the source travel time $\varphi(\underline{x},\underline{\eta})/c$. This gives the migrated image $O(\underline{x})$.

4) The reconstructed potential $\hat{U}(\underline{x})$ is given by (4.4), which is obtained by taking the gradient of $O(\underline{x})$ along the ray linking the source $\underline{\eta}$ to point $\underline{x}$, and by scaling the resulting expression with $n_0(\underline{x})/a(\underline{x},\underline{\xi})$.

The inversion procedure described above requires the computation of the extrapolated field $p_e(\underline{x},t)$ and the evaluation of the phase $\varphi(\underline{x},\underline{\eta})$ and amplitude $a(\underline{x},\underline{\eta})$ for all points in the medium. Since the location $\underline{\eta}$ of the source is fixed, this scheme requires the use of a ray tracing algorithm only for the source $\underline{\eta}$. By comparison, the inverse GRT [1]-[3] requires the use of a ray tracing procedure not only for $\underline{\eta}$, but also for every receiver $\underline{\xi}$ located along Γ. Our method can therefore be viewed as having replaced the use of a ray tracing scheme for receivers along Γ by the computation of $p_e(\underline{x},t)$, which can be done in one batch operation, instead of receiver by receiver. The advantages and disadvantages of our inversion method with respect to the inverse GRT are primarily those of finite difference schemes with respect to ray tracing methods. Thus, when the number of receivers is large, and when the finite-difference scheme which is used to compute $p_e(\underline{x},t)$ does not require too many grid points, our reconstruction technique is likely to be faster than the inverse GRT.

5. Characterization of the Cone $C(\underline{x})$

The accuracy of the reconstruction method which has been obtained in the

previous section depends in a crucial way on the angular aperture of the cone $C(\underline{x})$ appearing the representation (4.24) of the weighting function $M(\underline{x},\underline{x}')$. Indeed, as the angular aperture of $C(\underline{x})$ increases, within the approximations we have made $M(\underline{x},\underline{x}')$ gets closer to an impulse $\delta(\underline{x}-\underline{x}')$, and the Fourier transform $\hat{U}(\underline{p})$ of the reconstructed potential becomes a better approximation of the $U(\underline{p})$ in the high wavenumber region. We will show now that the angular range of $C(\underline{x})$ is purely a factor of the experiment geometry, and does not depend on the reconstruction technique that we have employed. In fact, as was already observed above, the same cone $C(\underline{x})$ appears also in the inverse GRT. Specifically, it will be shown that the angular range of $C(\underline{x})$ depends on the degree of coverage of the domain V which is provided by the receiver array Γ, and on the relative location of the source $\underline{\eta}$ with respect to point $\underline{x}$.

The first step is to note from (4.21) that $\nabla_{\underline{x}}\Phi(\underline{x},\underline{\xi})$ indicates the direction of a ray inside the cone $C(\underline{x})$, so that as $\underline{\xi}$ varies along Γ, $\nabla_{\underline{x}}\Phi(\underline{x},\underline{\xi})$ spans the cone $C(\underline{x})$, as shown in Fig. 4. The relation (4.9) also shows that $\nabla_{\underline{x}}\Phi(\underline{x},\underline{\xi})$ is the sum of the two vectors $\hat{u}(\underline{x},\underline{\xi})$ and $\hat{u}_i(\underline{x})$, which have the same length, and have angular arguments $\theta(\underline{x},\underline{\xi})$ and $\theta_i(\underline{x})$, respectively. Since $\hat{u}(\underline{x},\underline{\xi})$ and $\hat{u}_i(\underline{x})$ have the same length, the angle separating these two vectors is bisected by $\nabla_{\underline{x}}\Phi(\underline{x},\underline{\xi})$, as indicated in Fig. 5, so that the angular argument $\psi(\underline{x},\underline{\xi})$ of $\nabla_{\underline{x}}\Phi(\underline{x},\underline{\xi})$ is given by

$$\psi(\underline{x},\underline{\xi}) = \frac{1}{2}\left(\theta(\underline{x},\underline{\xi}) + \theta_i(\underline{x})\right) \quad . \tag{5.1}$$

Furthermore, since the source $\underline{\eta}$ is fixed, $\hat{u}_i(\underline{x})$ and therefore $\theta_i(\underline{x})$ are fixed, so that in (5.1) only $\theta(\underline{x},\underline{\xi})$ varies as $\underline{\xi}$ moves along Γ. Consequently, if we assume that $\theta(\underline{x},\underline{\xi})$ varies over the angular range $\Theta(\underline{x}) = [\theta_1(\underline{x}), \theta_2(\underline{x})]$ as $\underline{\xi}$

moves along Γ, the angular span of the cone $C(\underline{x})$ is

$$\Psi(\underline{x}) = [\tfrac{1}{2}(\theta_1(\underline{x}) + \theta_i(\underline{x})),\ \tfrac{1}{2}(\theta_2(\underline{x}) + \theta_i(\underline{x}))] \ . \qquad (5.2)$$

An interesting feature of this result is that the total aperture of $C(\underline{x})$ is $\frac{1}{2}$ $(\theta_2(\underline{x})-\theta_1(\underline{x}))$, which is half the range of $\Theta(\underline{x})$.

To interpret the above result, consider the special case when the background medium is constant. In this case, it is possible to determine more precisely the effect of the receiver array Γ on the span $\Psi(\underline{x})$ of $C(\underline{x})$. To do so, we will use for the array Γ a model of the type considered by Porter [20] and Esmersoy and Levy [16], where it is assumed that Γ is asymptotic to two lines wiht angles α_1 and α_2 with respect to the horizontal axis, as shown in Fig. 6. In exploration geophysics, this model covers the case when the scattered field is measured by receivers located on the surface of the earth ($\alpha_1 = 0$, $\alpha_2 = \pi$), or the offset vertical seismic profiling geometry, where the receivers are located on the surface of the earth and along a vertical borehole, say to the right of domain V ($\alpha_1 = \frac{\pi}{2}$, $\alpha_2 = \pi$), or even the case when the receivers are located above V and along two vertical boreholes on both sides of V ($\alpha_1 = \alpha_2 = \frac{\pi}{2}$).

Then, since the background medium is constant, the rays linking a point $\underline{x}$ in the medium to the source $\underline{\eta}$ and to receivers along Γ are straight lines. Thus, the angle $\theta_i(\underline{x})$ is the angle of the line from $\underline{\eta}$ to point $\underline{x}$, and by keeping track of the lines linking points along Γ to $\underline{x}$, we see that as $\underline{\xi}$ moves along Γ, $\hat{u}(\underline{x},\underline{\xi})$ sweeps a domain D illustrated in Fig. 6, whose angular range is $\Theta = [\alpha_2-\pi,\alpha_1+\pi]$. This angular range is independent of $\underline{x}$ and is completely parameterized by the angles α_1 and α_2 describing the array Γ. Consequently,

the range

$$\Psi(\underline{x}) = [\frac{1}{2}(\alpha_2 - \pi + \theta_i(\underline{x})) \ , \ \frac{1}{2}(\alpha_1 + \pi + \theta_i(\underline{x}))] \qquad (5.3)$$

of cone $C(\underline{x})$ is purely a factor of the experiment geometry, and depends on $\underline{x}$ only through the angle $\theta_i(\underline{x})$ describing the relative location of the source $\underline{\eta}$ and point $\underline{x}$.

The last point that needs to be clarified is the effect of the high frequency constraint $|k| \geq r$ on the range of values of the wavevector $\underline{p}$ under the transformation (4.21). As indicated at the end of section 4, in this case $\underline{p} \in C_r(\underline{x})$ where $C_r(\underline{x})$ is obtained by subtracting from the cone $C(\underline{x})$ a set located in the vicinity of $\underline{p} = 0$. To characterize this set, note from (4.21) that

$$p = |\underline{p}| = |k| \ |\nabla_{\underline{x}} \Phi(\underline{x}, \underline{\xi})| \ , \qquad (5.4)$$

and taking into account the fact that the vector $\nabla_{\underline{x}} \Phi(\underline{x}, \underline{\xi})$ is the sum of the vectors $\hat{u}(\underline{x}, \underline{\xi})$ and $\hat{u}_i(\underline{x})$ which have the same length $n_0(\underline{x})$, we find that

$$|\nabla_{\underline{x}} \Phi(\underline{x}, \underline{\xi})| = 2n_0(\underline{x}) \cos((\theta(\underline{x}, \underline{\xi}) - \theta_i(\underline{x}))/2) \qquad (5.5)$$

Thus, in the direction $\psi(\underline{x}, \underline{\xi}) = (\theta(\underline{x}, \underline{\xi}) + \theta_i(\underline{x}))/2$, the wavevector $\underline{p}$ must be such that

$$p \geq 2rn_0(x) \cos((\theta(\underline{x}, \underline{\xi}) - \theta_i(\underline{x}))/2) = 2rn_0(x) \cos(\psi - \theta_i(x)) \ . \qquad (5.6)$$

But $p = 2rn_0(\underline{x}) \cos(\psi - \theta_i(\underline{x}))$ is the equation of a circle centered at $r\hat{u}_i(\underline{x})$ and of radius $rn_0(\underline{x})$. This shows that $C_r(\underline{x})$ is obtained by subtracting from the cone $C(\underline{x})$ the points which are inside a disk of radius $rn_0(\underline{x})$ centered at $r\hat{u}_i(\underline{x})$, or which are inside the symmetric image of this disk with respect to the origin, as indicated in Fig. 7.

An interesting aspect of the above result is that when $\psi = \theta_i(\underline{x}) + \frac{\pi}{2}$, which

corresponds to the case where $\theta(\underline{x},\underline{\xi}) = \theta_i(\underline{x})+\pi$, or equivalently $\hat{u}(\underline{x},\underline{\xi}) = -\hat{u}_i(\underline{x})$, then the origin $\underline{0}$ belongs to the domain $C_r(\underline{x})$. This indicates that some coverage in the low wavenumber region is possible for certain source-receiver geometries. Note that when $\hat{u}(\underline{x},\underline{\xi}) = -\hat{u}_i(\underline{x})$, the receiver $\underline{\xi}$ is located on the other side of V with respect to the source $\underline{\eta}$, but on the same ray. This geometry is of a tomographic nature, and arises in exploration geophysics for vertical seismic profiling or borehole to borehole surveys, where in the last case the source and receivers are located in two different vertical boreholes. By comparison, note that when $\psi = \theta_i(\underline{x})$, which corresponds to $\theta(\underline{x},\underline{\xi}) = \theta_i(\underline{x})$ and $\hat{u}(\underline{x},\underline{\xi}) = -\hat{u}_i(\underline{x})$, the wavenumber p must be such that $p \geq 2rn_0(\underline{x})$, and $\underline{p}$ is therefore bounded away from zero. This special case corresponds to the so-called zero-offset experiment geometry, where the source and receiver coincide. Such a geometry can be used as a model for surface surveys in exploration geophysics, where the source and receivers are located on the surface of the earth at relatively small distance from each other. The above observations indicate that in order to gain some information about the slow space variations of the scattering potential $U(\underline{x})$, a tomographic experiment geometry must be employed.

6. Conclusion

In this paper, we have obtained a new solution to the variable background Born inversion problem for the case when the medium is probed by a single point source. This solution generalizes a reconstruction technique proposed earlier by Esmersoy [14] for the constant background case. In our reconstruction method, the backpropagated field $p_e(\underline{x},t)$ is first computed by a finite difference sheme, and is imaged at the source travel times. This gives the migrated image $O(\underline{x})$, and by taking the gradient of this image along rays linking the source to every point in the medium, and scaling the resulting image appropriately, we obtain the reconstructed potential $U(\underline{x})$. When the receiver array provides a total coverage of the domain where the scattering potential $U(\underline{x})$ is concentrated, the reconstructed potential recovers exactly the rapid space variations of $U(\underline{x})$, or equivalently the high wavenumber part of its Fourier transform. In general, within several approximations which restrict the validity of our reconstruction procedure to the high wavenumber region, it is shown that $\hat{U}(\underline{x})$ corresponds to the convolution at point $\underline{x}$ of $U(\bullet)$ with a weighting function obtained by reconstructing an impulse from its projections over a cone $C(\underline{x})$. The angular range of the cone $C(\underline{x})$ depends only on the experiment geometry, and not on the reconstruction method that we have employed.

The most significant computational requirement of the procedure described above is the computation of the extrapolated field $p_e(\underline{x},t)$ with a finite-difference scheme. By comparison, the generalized Radon transform inversion method [1]-[3] requires the use of a ray tracing scheme, and the

evaluation of the phase and amplitude along each ray, for every receiver along the receiver array Γ. We expect therefore that, for a wide class of problems, our method will be faster than the inverse GRT but a detailed comparison of the relative efficiency of these two techniques will be necessary. A number of factors are likely to influence this comparison. The first factor is the number of receivers along Γ: clearly, as this number grows, the numerical complexity of the inverse GRT increases significantly, whereas the number of operations required to compute the backpropagated field $p_e(\underline{x},t)$ remains approximately the same. Another factor is the complexity of the background refraction index profile $n_0(\bullet)$. It is known that ray tracing schemes perform very well for simple media, but are relatively inaccurate, and difficult to use for complex media. By comparison, the finite-difference method is a brute force technique which is not affected significantly by the complexity of the background profile $n_0(\bullet)$. Finally, another important factor in our comparison will be the relative location of the domain V that we want to image with respect to the receiver array Γ. If this domain is not too far away from Γ, the finite-difference technique is relatively easy to use, since it does not require the computation of $p_e(\underline{x},t)$ over a very large region of space. However, if V is far away from Γ, the finite-difference technique becomes very slow, whereas the ray tracing approach is not significantly affected by the increase in size of the domain that we consider. The above observations seem to suggest that the inverse GRT and the method that we propose here are almost complementary, in the sense that one method will perform best on problems for which the other is least suited. However, these conclusions are rather tentative, since as mentioned above, a detailed comparison of these two

methods has yet to be performed. Note that our reconstruction technique gives good results in the constant background case [14].

Several assumptions have been made throughout this paper. The first of these is that the medium that we consider is two-dimensional. The reconstruction procedure which has been presented above can be extended in a straightforward way to 3-D media. Another significant restriction which has been imposed is that the background refraction index $n_0(\bullet)$ is a smooth function. This assumption is somewhat unrealistic in practice, since most geological structures exhibit significant discontinuities. It would therefore be of interest to extend our reconstruction technique to the case when the background index $n_0(\bullet)$ is discontinuous. The main difficulty in this context is that at interfaces where $n_0(\bullet)$ is discontinuous, the incident waves are partly reflected, so that multiply reflected waves exist, and in this case the asymptotic form (2.8) of the Green's function is not valid. If the reflected waves are neglected, and if only the transmission losses at interfaces are taken into account, it was shown in [1] how to reconstruct $U(\bullet)$. However, it would be ultimately desirable to obtain a reconstruction technique that takes into account the reflected waves appearing in the background model. In addition, we note that our reconstruction technique applies only to before stack data, i.e. to data collected from a single experiment. In actual geophysical surveys, several experiments are carried out for different source and receiver locations. It would therefore be useful to find a way of combining the reconstructed potentials $\hat{U}_i(\underline{x})$, $1 \leq i \leq k$ obtained for several experiments, where k is the number of experiments. Note that in this case the cones $C_i(\underline{x})$, $1 \leq i \leq k$ at a point $\underline{x}$ will provide different angular coverages

for different experiment geometries. A simple averaging of the potentials $\hat{U}_i(\underline{x})$ does not give a satisfactory solution to this problem, since this average would have for effect to weight too heavily the regions where the cones $C_i(\underline{x})$ overlap. Another way of formulating this problem is to consider the zero-offset geometry, where the data is given for coincident source-receiver pairs located along a curved array. This data is obtained by applying the common depth point (CDP) stacking process [23] to the data collected from a large number of experiments. For a 2 1/2-D zero-offset geometry, and when the background refraction index is constant, an inversion technique which relies on the backpropagated field was proposed by Esmersoy [14]. We expect that this inversion technique can be extended to the variable background case by using ideas similar to those that have been discussed in this paper.

Acknowledgement: The authors wish to thank an anonymous referee for suggesting several improvements in an earlier version of this paper, and in particular for pointing out the proof which has been used in section 3 to show that for high frequencies, the definitions (3.1) and (3.11) of the extrapolated field are equivalent.

References

[1] G. Beylkin, "Imaging of discontinuities in the inverse scattering problem by inversion of a causal generalized Radon transform," J. Math. Phys., Vol. 26, No. 1, pp. 99-108, January 1985.

[2] D. Miller, M. Oristaglio and G. Beylkin, "A new formalism and old heuristic for seismic migration," Extended Abstracts, 54th Annual

International Meeting of the Society of Exploration Geophysicists, Atlanta, 1984, pp. 704-707.

[3] D. Miller, M. Oristaglio and G. Beylkin, "A new slant on seismic imaging: Classical migration and integral geometry," Research Note, Schlumberger-Doll Research, Jan. 1986.

[4] R.H. Stolt and A.B. Weglein, "Migration and inversion of seismic data," Geophysics, Vol. 50, No. 12, pp. 2458-2472, December 1985.

[5] S.J. Norton and M. Linzer, "Ultrasonic reflectivity imaging in three dimensions: Exact inverse scattering solutions for plane, cylindrical, and spherical apertures," IEEE Trans. Biomedical Eng., Vol. BME-28, No. 2, 202-220, February 1981.

[6] K.P. Bube and R. Burridge, "The one-dimensional problem of reflection seismology," SIAM Review, Vol. 25, No. 4, pp. 497-559, October 1983.

[7] G. Beylkin and M.L. Oristaglio, "Distorted-wave Born and distorted-wave Rytov approximations," Optics Communications, Vol. 53, No. 4, pp. 213-216, March 1985.

[8] J.K. Cohen and N. Bleistein, "Velocity inversion procedure for acoustic waves," Geohysics, Vol. 44, No. 6, pp 1077-1087, June 1979.

[9] J.A. Fawcett, "Inversion of N-dimensional spherical averages," SIAM J. Applied Math., Vol. 45, No. 2, pp. 336-341, April 1985.

[10] N. Bleistein and S.H. Gray, "An extension of the Born inversion method to a depth dependent reference profile," Geophysical Prospecting, Vol. 33, No. 7, pp. 999-1022, November 1985.

[11] J.K. Cohen and F.G. Hagin, "Velocity inversion using a stratified reference," Geophysics, Vol. 50, No. 11, pp. 1689-1700, November 1985.

[12] S. Raz, "Three-dimensional velocity profile inversion from finite-offset scattering data," Geophysics, Vol. 46, No. 6, pp. 837-842, June 1981.

[13] R.W. Clayton and R.H. Stolt, "A Born-WKBJ inversion method for acoustic reflection data," Geophysics, Vol. 46, no. 11, pp. 1559-1567, November 1981.

[14] C. Esmersoy, "The backpropagated field approach to multidimensional velocity inversion," Ph.D. thesis, Department of Electrical Engineering and Computer Science, MIT, November 1985.

[15] C. Esmersoy, M.L. Oristaglio and B.C. Levy, "Multidimensional Born velocity inversion: Single wide-band point source," J. Acoustical Soc. America, Vol. 78, No. 3, pp. 1052-1057, September 1985.

[16] C. Esmersoy and B.C. Levy, "Multidimensional Born inversion with a wide-band plane wave-source," Proc. IEEE, special issue on seismic inversion, Vol. 74, No. 3,pp. 466-475, March 1986.

[17] N. Bleistein, J.K. Cohen and F.G. Hagin, "Two-and-one-half dimensional Born inversion with an arbitrary reference", Report CWP-032, Center for Wave Phenomena, Colorado School of Mines, Golden, CO, October 1985.

[18] J.R. Taylor, Scattering Theory, John Wiley and Sons, Inc., New York, 1972.

[19] P.M. Morse and H. Feshbach, Methods of Theoretical Physics, parts I and II, McGraw-Hill, New York, 1953.

[20] R.P. Porter, "Diffraction-limited, scalar image formation with holograms of arbitrary shape," J. Optical Soc. America, Vol. 60, No. 8, pp. 1051-1059, August 1970.

[21] N.N. Bojarski, "A survey of the near-field far-field inverse scattering inverse source integral equation," IEEE Trans. Antennas and Propagation, Vol. AP-30, No. 5, pp. 975-979, September 1982.

[22] A.J. Berkhout, Seismic Migration-Imaging of Acoustic Energy by Wave Field Extrapolation, 2nd edition, Elsevier, Amsterdam, 1982.

[23] G.H.F. Gardner, editor, Migration of Seismic Data, Geophysics reprint series, No. 4, Society of Exploration Geophysicists, Tulsa, Oklahoma, 1985.

[24] J.F. Claerbout, Imaging the Earth's Interior, Blackwell Scientific Publications, Oxford, England 1985.

[25] R.M. Alford, K.R. Kelly and D.M. Boore, "Accuracy of finite-difference modeling of the acoustic wave equation," Geophysics, Vol. 39, No. 6, pp. 834-842, December 1974.

[26] W-F. Chang and G.A. McMechan, "Reverse-time migration of offset vertical seismic profiling data using the excitation-time imaging condition," Geophysics, Vol. 51, No. 1, pp. 67-84, January 1986.

[27] J.B. Keller, "Rays, waves and asymptotics," Bull. Amer. Math. Soc., Vol. 84, No. 5, pp. 727-751, September 1978.

Figure Captions

Figure 1: Scattering experiment. The medium is probed by an impulsive point source located at $\underline{\eta}$ and the scattered field is observed along the receiver array Γ.

Figure 2: Parametrization of the rays linking point $\underline{x}$ to the source $\underline{\eta}$ and to receiver $\underline{\xi}$. The doublet sources generating the backpropated field are indicated by + and - signs.

Figure 3: Infinitesimal ray tube originating from point $\underline{x}$ and centered around the ray linking $\underline{x}$ to receiver $\underline{\xi}$.

Figure 4: Cone $C(\underline{x})$ spanned by $\nabla_{\underline{x}}\Phi(\underline{x},\underline{\xi})$ as $\underline{\xi}$ moves along Γ.

Figure 5: Construction of $\nabla_{\underline{x}}\Phi(\underline{x},\underline{\xi})$ by summation of the vectors $\hat{u}(\underline{x},\underline{\xi})$ and $\hat{u}_i(\underline{x})$.

Figure 6: Receiver array with angular aperture $[\alpha_1, \alpha_2]$. D denotes the domain swept by the vector $\hat{u}(\underline{x},\underline{\xi})$ as $\underline{\xi}$ moves along Γ.

Figure 7: Range $C_r(\underline{x})$ of the wavevector $\underline{p}$ under the high frequency constraint $|k| \geq r$.

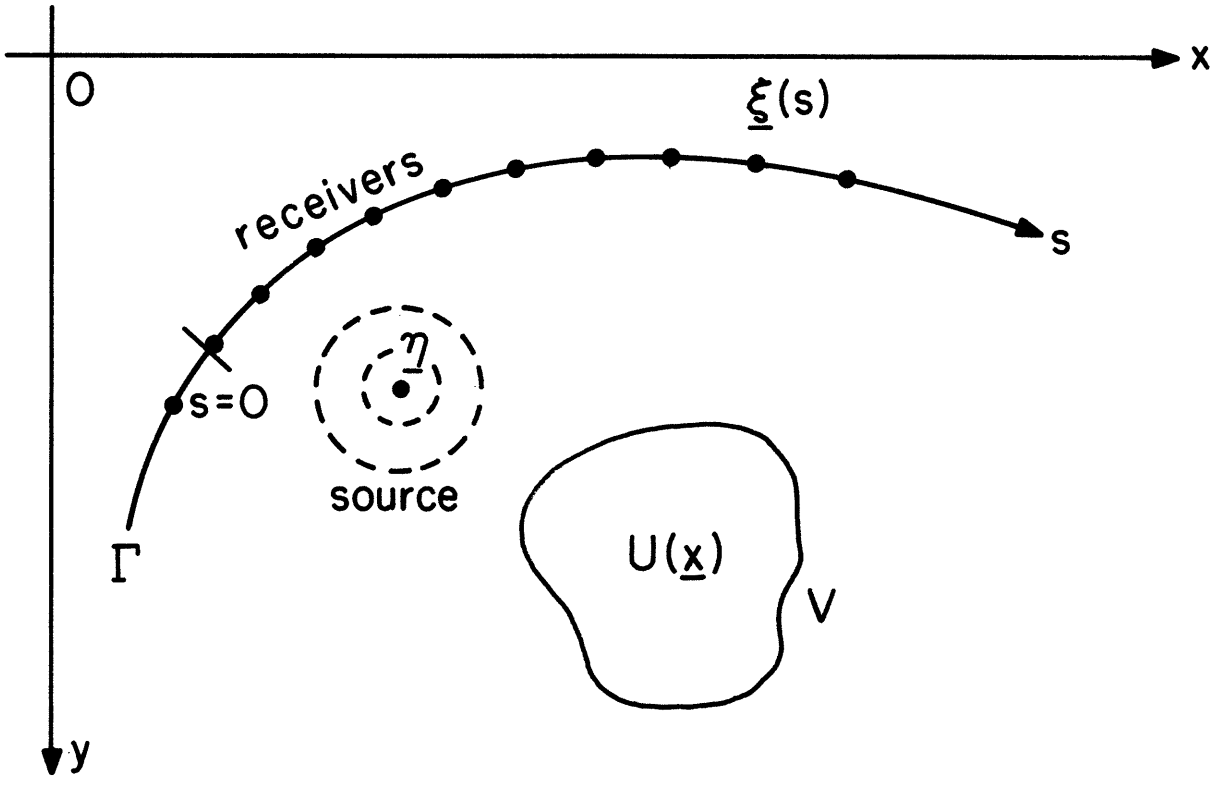
x
O
$\underline{\xi}(s)$
receivers
s
η
s=O
source
Γ
U($\underline{x}$)
V
y

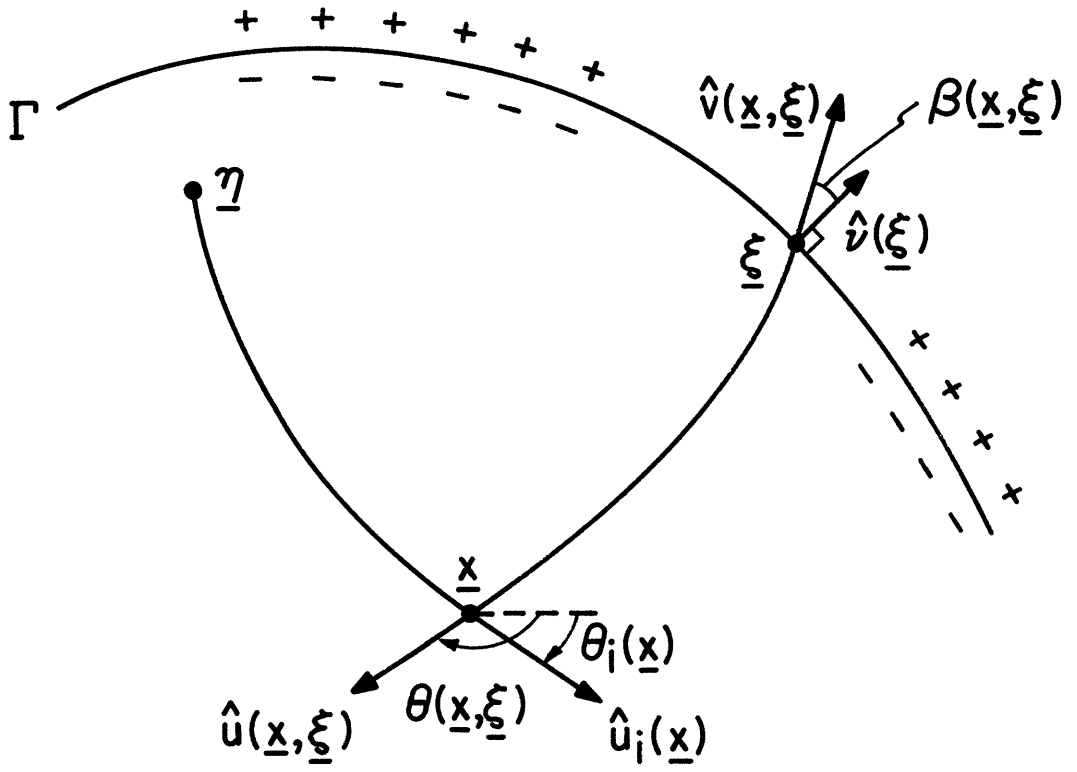
Γ
η
ξ
x
$\hat{v}(x,\xi)$
$\beta(x,\xi)$
$\hat{v}(\xi)$
$\theta_i(x)$
$\theta(x,\xi)$
$\hat{u}(x,\xi)$
$\hat{u}_i(x)$

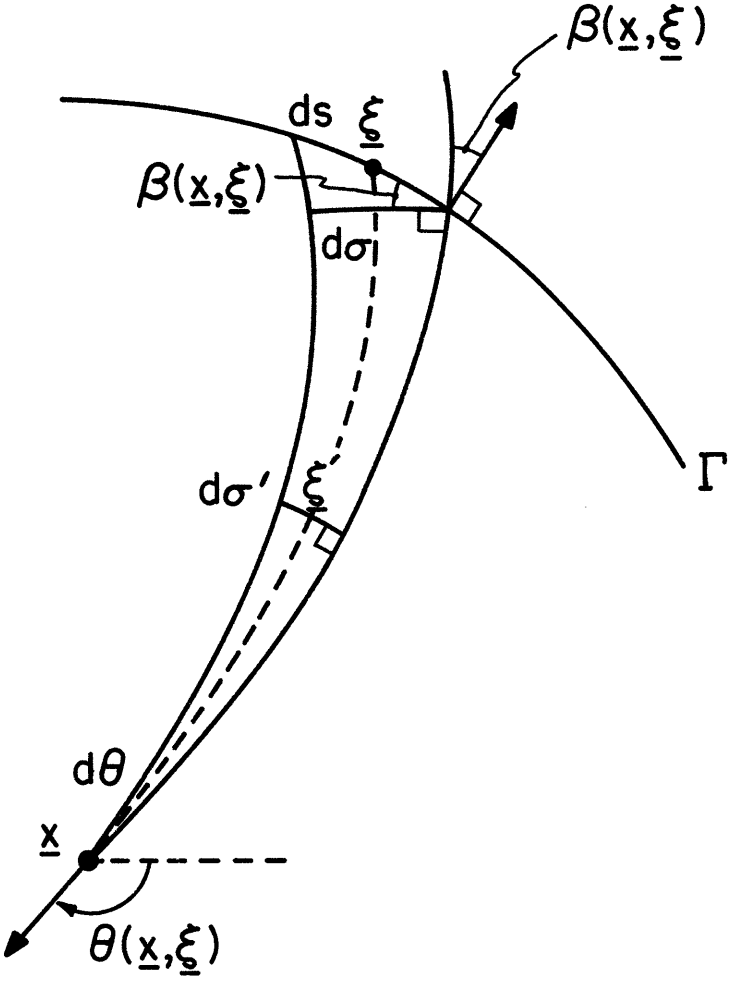
β(x,ξ)
ds ξ
β(x,ξ)
dσ
dσ'
ξ
Γ
dθ
x
θ(x,ξ)

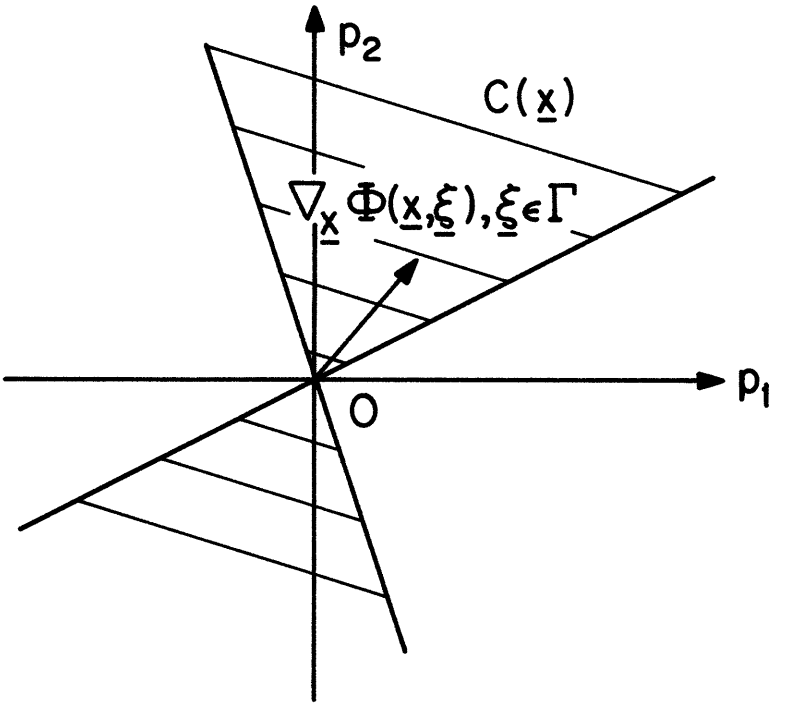

FIG. 4

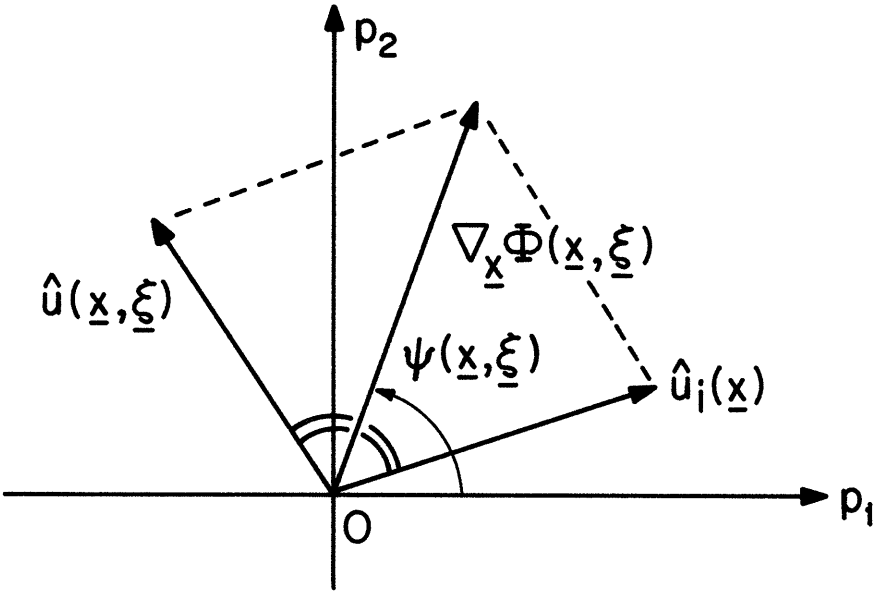

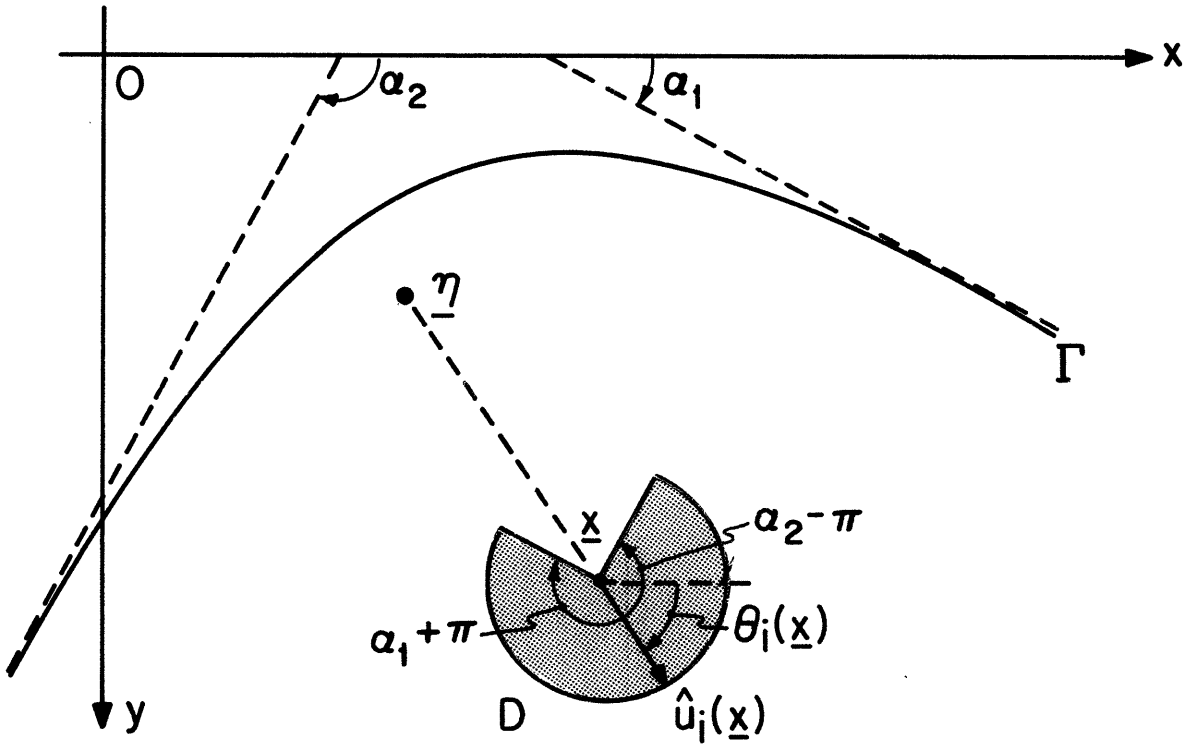
x
O
α_2
α_1
$\underline{\eta}$
Γ
$\underline{x}$
$\alpha_2 - \pi$
$\alpha_1 + \pi$
$\theta_i(\underline{x})$
y
D
$\hat{u}_i(\underline{x})$

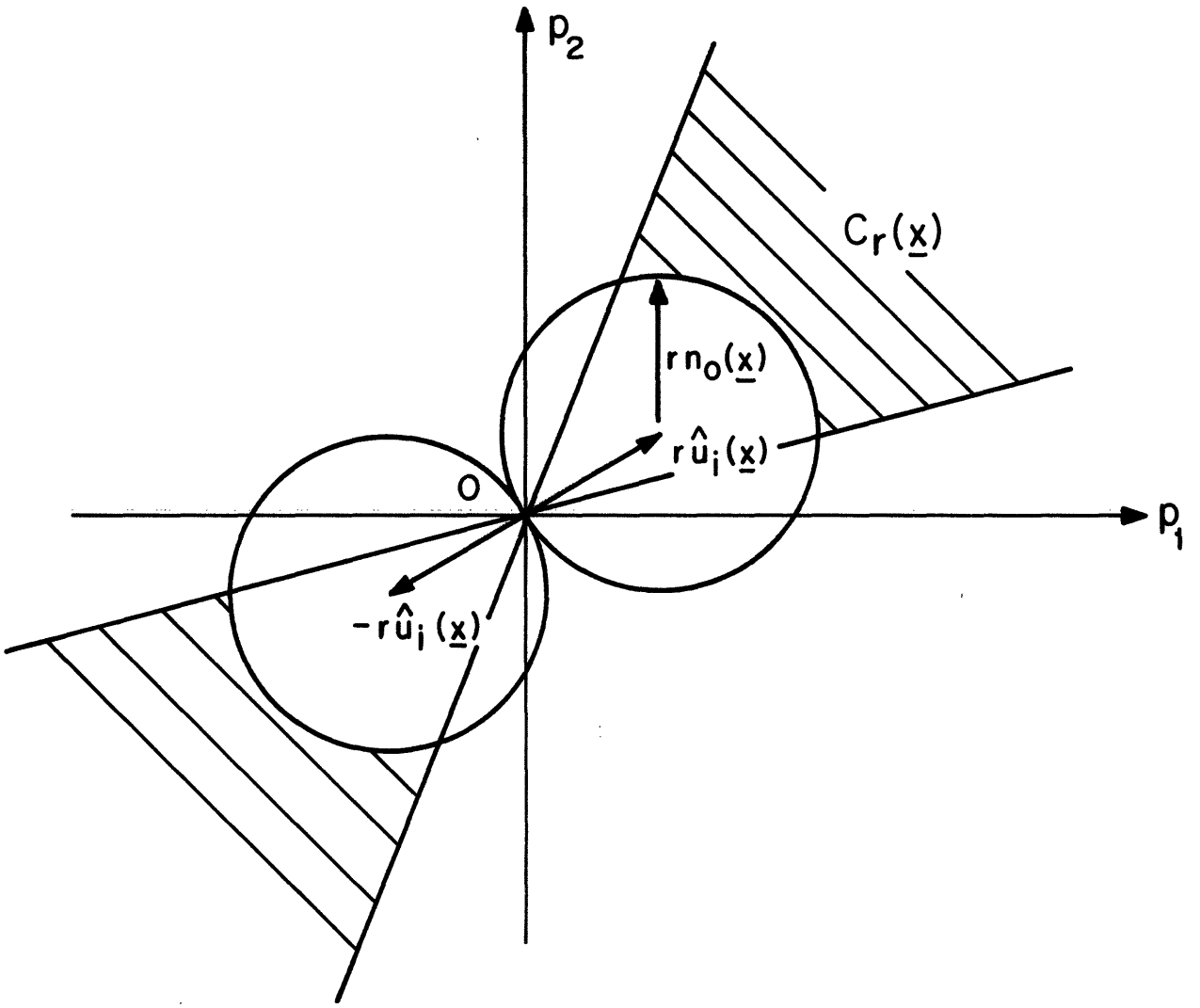
p_2
$C_r(\underline{x})$
$r\,n_o(\underline{x})$
$r\,\hat{u}_i(\underline{x})$
0
p_1
$-r\,\hat{u}_i(\underline{x})$